https://doi.org/10.5194/egusphere-2026-4631
Preprint. Discussion started: 7 August 2026

Derivation of the multi-Doppler 3D wind field during the 2023 WesCon-WOEST campaign in southern England

Robert J. Thompson[1], Thorwald H. M. Stein[1], Chun Hay Brian. Lo[1], Robert Jackson[2], Christopher D. Westbrook[1], Scott Collis[2], Lindsay Rhodes[3,4], Timothy Darlington[5], Emily G. Norton[6], Paul A. Barrett[5], and Ryan R. Neely III[3,4]

[1]Department of Meteorology, University of Reading, Reading, UK
[2]Argonne National Laboratory, Argonne, IL, US
[3]National Centre for Atmospheric Science, Leeds LS2 9PH, UK
[4]School of Earth, Environment and Sustainability, University of Leeds, Leeds LS2 9JT, UK
[5]Met Office, Exeter, UK
[6]NCAS, University of Manchester, UK

Correspondence: Robert J. Thompson r.j.thompson@reading.ac.uk Thorwald H. M. Stein t.h.m.stein@reading.ac.uk

Abstract. Convection drives high-impact weather events but remains challenging to represent accurately in modern convection-resolving weather prediction models. Robust evaluation and development of these models therefore require detailed observations of convective dynamics, with enough data for statistical application. In this study we present the first multi-Doppler radar 3D wind analysis in the UK. Five radars used in the WesCON-WOEST field campaign are used with an updated version of the PyDDA algorithm. This includes a newly implemented "ORIGAMI" unfolding algorithm based on model winds, a combined VAD initialisation and a cloud-top boundary condition. The resulting dataset provides a complete 3D wind grid with 1 km horizontal and 500 m vertical resolution every 10 minutes over the 3 month field campaign. Validation against two radar wind profilers show the horizontal wind components have RMSE better than $2.4\ \mathrm{ms}^{-1}$, with a small bias in the westerly component, u. Statistical comparison to aircraft flight data shows similar distribution, but underestimates the strongest up- and downdrafts, as a result of not resolving the scale of the smallest updrafts. This data provides important dynamical information on convective processes and offers a valuable resource for evaluating and improving convection-resolving models.

1 Introduction

Convection plays a central role in driving hazardous weather, including heavy rainfall, strong winds, and hail. Understanding and representing the internal dynamics of convective weather systems remains a critical challenge to improving weather forecasts and nowcasts. Numerical weather prediction (NWP) models are increasingly run operationally on the kilometer scale (Clark et al., 2016) and sub-km horizontal grid spacing, allowing the explicit simulation of individual updrafts. The development of such models also highlights the need to match high-resolution observational datasets for validation and verification (Schär et al., 2020). Here, we present a 3D wind field derived from Doppler radars for the WesCon-WOEST campaign that took place in southern England in 2023 (Barr et al., 2026), generated to evaluate future sub-km NWP models.

https://doi.org/10.5194/egusphere-2026-4631
Preprint. Discussion started: 7 August 2026

Doppler weather radar provides one of the most effective remote sensing tools for measuring cloud, rainfall, and winds (in the presence of targets) at high spatial and temporal resolution. Gridded products for rainfall are commonplace worldwide; in the UK, the rainfall radar composite (Harrison et al., 2009) provides real-time guidance and is used for studying flooding (Roberts et al., 2009), climate effects (Fairman Jr et al., 2017; Lengfeld et al., 2020) and model evaluation (Hanley et al., 2015; Stein et al., 2014; Mittermaier, 2014). The development of a 3D gridded reflectivity composite (Scovell and Al-Sakka, 2016) has unlocked the potential of radar observations to capture convective storm development including for model evaluation (Stein et al., 2020; Field et al., 2023; Lo et al., 2024). However, operational radar networks have been designed for maximum coverage for rainfall estimation, lacking the density to enable multi-Doppler wind estimates that require observation by multiple radars at differing angles.

A Doppler radar measures only the radial component of the wind, leaving the full wind vector under-determined. Combining radial velocity data from Doppler radars at different locations enables the retrieval of horizontal and vertical wind components, demonstrated as early as the 1970s (Lhermitte and Miller, 1970; Lhermitte, 1970). Various approaches and software products are currently available to generate 3D winds from multiple radars on a common grid. Gao et al. (1999, 2004) proposed a variational approach to multi-Doppler analysis including mass continuity and vertical vorticity constraints have since been introduced (e.g. Liou and Chang, 2009). Schemes currently used in the community include "SAMURAI" (Bell et al., 2012), "WISSDOM" (Tsai et al., 2023), and "MultiDop" (Potvin et al., 2012b) furthered by Lang et al. (2017), which has then been incorporated into a system called PyDDA (Jackson et al., 2020). Examples of Multi-Doppler successfully implemented are a study of organised convection in the Southern Great Plains (North et al., 2017), use of SAMURAI for convection over complex terrain in northern Spain (del Moral et al., 2020) and PyDDA implemented for WSR-88D radar pairs for the GPM validation Network (Gatlin et al., 2020). Similarly, a nationwide multi-Doppler product was developed over France by Bousquet and Tabary (2014), initially at 2.5 km horizontal and 500m vertical resolution, and has been demonstrated to accurately reveal model errors (Beck et al., 2014) and support case studies of severe convection (Ribaud et al., 2016).

In the United Kingdom, the radar network was upgraded to have full Doppler (using split PRF) and dual-polarisation capability between 2011–2018. Although this has made dual-Doppler case studies possible (Westbrook and Clark, 2013), a multi-Doppler product has not been attempted, partly due to the distance between the radars. The WesCon-WOEST campaign data used in this study complemented the operational UK radar network with two X-band radars as well as the Met Office research radar at Wardon Hill, presenting a unique opportunity for 3D wind retrieval in the UK. When considering multi-Doppler retrievals to study convection, a particular challenge for the UK is that convection is often weakly forced, transient, and small scale, meaning that the target grid scale for a multi-Doppler composite should be no greater than 1 km. This is achievable for the WesCon-WOEST campaign as the radars all have significantly better resolution than this requirement,

In this paper we describe the first multi-Doppler wind estimates in the UK, with 1 km horizontal and 500m vertical resolution over a region spanning a 189 × 132 km domain at 10-minute intervals. The primary motivation is to provide physically-plausible estimates of updraft strength and sizes to constrain sub-km NWP simulations. To achieve this we introduce a new Doppler unfolding algorithm, ORIGAMI, and an additional boundary condition to the variational solver, to avoid spurious above-cloud vertical velocities. The manuscript is organised as follows: In Section 2, we briefly introduce the WesCon-WOEST campaign

https://doi.org/10.5194/egusphere-2026-4631
Preprint. Discussion started: 7 August 2026

and the radar data, as well as other data sets used. In Section 3 we cover necessary radar data processing techniques, the PyDDA retrieval method, and our adaptations of PyDDA. Verification of the 3D winds against radar wind profiler measurements is considered in Section 4 with sensitivity tested in section 5. We provide a number of examples of successfully derived wind fields in Section 6. We discuss challenges in verification of the vertical wind against aircraft measurements and other radar-derived estimates in Section 7 before presenting our conclusions in Section 8.

2 Data

2.1 WesCon-WOEST

The data used in this work is from the WesCon-WOEST project (Barr et al., 2026), which took place in summer 2023 in southern England. The campaign forms part of the ParaChute programme (https://www.metoffice.gov.uk/research/approach/collaboration/parachute) set up to improve the representation of convection and turbulent processes in sub-km NWP models. The campaign focus was on the convective boundary layer and convective storms, featuring several scanning radars, two aircraft, uncrewed aerial systems, and many complementary ground-based observations. The campaign included 30 intensive observation periods (IOP), of which 17 days included aircraft operations, and 17 days with real-time radar tracking of convective storms. The radars used in this study were scanning operationally, meaning that 3D winds may be generated for the entire campaign period from 1 June to 31 August 2023. The availability of aircraft and research radar observations during the IOPs provides both an opportunity to create the 3D wind dataset, but also increases the potential for multi-platform analyses of convective storms. The full operational use provides a dataset suitable for statistical model evaluation rather than being purely case study based.

2.2 Scanning radars

Two mobile X-band radars, NXPol-1 and NXPol-2 (Neely III et al., 2018), were located approximately 60 km apart at Lyneham ($51.507\,°$N, $2.005\,°$W), and Chilbolton ($51.145\,°$N, $1.439\,°$W), respectively. The two radars complemented the C-Band radars operated by the Met Office, including those in the UK operational radar network (Darlington, 2015) and the Wardon Hill radar ($50.818\,°$N, $2.555\,°$W) used for research purposes. Only the network radars located at Cobbacombe ($50.963\,°$N, $3.451\,°$W) and Dean Hill ($51.030\,°$N, $1.653\,°$W) are included in our 3D wind composite as they cover a sufficient part of the target region. Table 1 summarises the parameters from these radars that are relevant to the Doppler measurements and their locations are shown in Figure 1(a).

The two NXPol radars and the Wardon Hill radar operated a 10-minute scan strategy during WesCon-WOEST, alternating between a convective mode and a boundary-layer mode which is not considered in this study. During the convective mode, the NXPol radars carried out 12 plan-position indicator scans (PPIs) with elevations $1.5°$, $2.5°$, $3.5°$, $4.5°$, $5.5°$, $7.0°$, $8.5°$, $10.0°$, $11.5°$, $13.0°$, $14.5°$ and $17.0°$. In addition data from three nearby radars operated by the Met Office are used (Met Office, 2003). The Wardon Hill radar carried out 10 PPIs at $1.0°$, $2.0°$, $3.0°$, $4.0°$, $5.0°$, $6.5°$, $8.0°$, $9.5°$, $11.0°$ and $12.5°$ elevations.

https://doi.org/10.5194/egusphere-2026-4631
Preprint. Discussion started: 7 August 2026

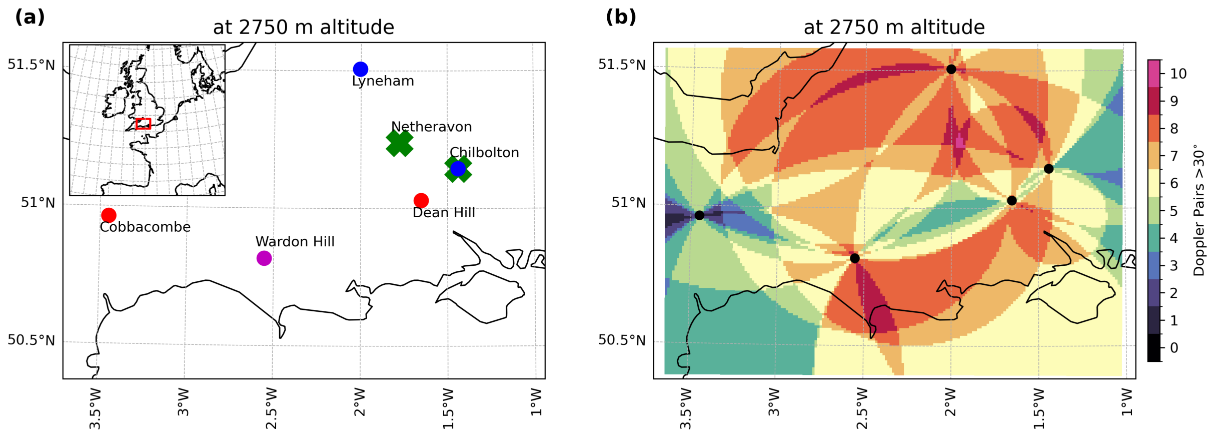

Figure 1. (a) Map of the Wessex region in the southern UK showing the locations of radars (circles) and radar wind profilers (crosses) used in this study, inset is a map that places the region in the context of Western Europe. (b) Number of Doppler radar pairs with at least 30° angle between beams.

Radars	**NXPol**	**Met Office Wardon Hill**	**Met Office Operational**	**CAMRa**
Locations	Lyneham, Chilbolton	Wardon Hill	Cobbacombe, Dean Hill	Chilbolton
Frequency/Band	9.3 GHz / X	5.6 GHz / C	5.6 GHz / C	3.0 GHz / S
Unambiguous Range (km)	100	125	125	246
Max Digitised Range (km)	98	113	113	199
Beamwidth to -3 dB ($^\circ$)	1.0	1.1	1.1	0.28
Strategy	12 PPI	10 PPI	5 PPI	RHIs (*)
Maximum Elevation ($^\circ$)	17	12.5	9	90
Nyquist Velocity (m s^{-1})	12	48	48	15

Table 1. List of parameters relevant for Doppler measurements for each of the radars used in this study. "Strategy" refers to the number of Doppler-suitable scans available for 3D wind generation, each 10 minute cycle, with maximum elevation being the highest available of those scans (see main text for details of the individual elevation angles. (*) The azimuths and elevation angles for the CAMRa RHIs were determined in real-time using a cell-tracking algorithm (Stein et al., 2015).

https://doi.org/10.5194/egusphere-2026-4631
Preprint. Discussion started: 7 August 2026

The Cobbacombe and Dean Hill radars carried out their standard operating procedure, which includes five PPIs specifically optimised for Doppler measurements at elevations of 1.0°, 2.0°, 4.0°, 6.0° and 9.0°; these Doppler scans were also made every 10 minutes.

Figure 1's right panel shows where in the region dual- or multi-Doppler wind retrievals are possible based on an angle between 30–150°, to give angles suitably different for deriving 2 components (note that the so-called "cone of silence" is not considered to keep the figure legible). Combined, these five radars provide excellent coverage of the target region, particularly in the area between 3–2 °W where most of the research flights took place.

2.2.1 Doppler quality control

For generation of a useful 3D wind field, we must apply a quality control procedure, as erroneous observations would lead to artificial flows. That means that we must remove noisy Doppler measurements from our radar data, but also areas which provide data that is otherwise unreliable, notably ground clutter and blocked beams.

To ensure good quality Doppler data a radial velocity texture is calculated based on the standard deviation of 3 by 3 pixels at each point. This texture gives an excellent separation of good data from hydrometeors and noisy data with weak signals, or otherwise unreliable data due to rapidly changing velocities, see Figure 2. A radar-dependent texture limit is applied, with any velocity where texture is greater than this limit being discounted from further analysis, using 3 ms^{-1} for the NXPol radars and 5 $\mathrm{m\ s}^{-1}$ for the Met Office radars. This limit is selected empirically from histograms such as figure 2, though there is little sensitivity to the value as long as it comfortably partitions the peaks of the distribution. We find that this procedure also removes rays where blocking is enough to degrade the data, which will be a result of the reduced reflectivity reducing the signal to noise ratio in significantly blocked beams.

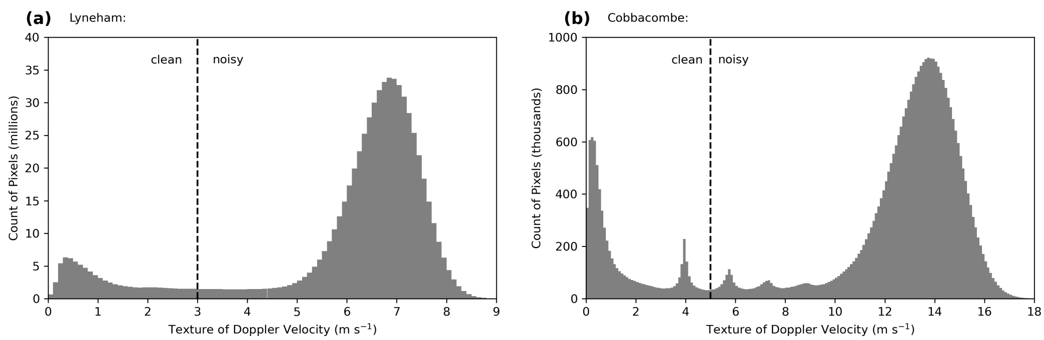

Figure 2. (a) Velocity texture filter on the NXPol radar at Lyneham, demonstrating the clear distinction between clean and noisy data. This histogram is of all data from all radar volumes on 3rd August 2023, of the Lyneham X-band radar. The dashed vertical line shows the 3 $\mathrm{m\ s}^{-1}$ texture limit. (b) The same but for the Met Office radar at Cobbacombe and using a 5 $\mathrm{m\ s}^{-1}$ texture limit.

https://doi.org/10.5194/egusphere-2026-4631
Preprint. Discussion started: 7 August 2026

2.2.2 CAMRa

The Chilbolton Advanced Meteorological Radar (CAMRa) was operated on 17 IOP days. A clear-air strategy was usually carried out early in the day and included a PPI at low elevation followed by a set of RHIs at pre-determined azimuths; this cycle took 30 minutes to complete. When convective storms were within 100 km of Chilbolton, an automated track-and-scan procedure was carried out, targeting individual convective storms and sampling their cores with repeated sets of RHI scans. While the CAMRa scans are not included in the multi-Doppler retrieval in this study, they provide a valuable data set for verification. CAMRa has a 0.28° beam width and was operated with 75-m range gates. The RHIs were configured to capture the entire depth of the targeted convective storm. As such, the CAMRa RHIs allow us to investigate the limitations of the multi-Doppler retrieval due to resolution as well as due to poorer sampling of the upper troposphere, not as an independent "truth," but as a scale-consistent structural comparison for narrow updraft features.

2.3 Radar wind profilers

Radar wind profilers (RWPs), also referred to as Doppler radars, boundary layer wind profilers or UHF wind profilers in the literature, are widely used by meteorological services to obtain continuous vertical profiles of the three wind components (u, v, w).

RWPs derive wind information by measuring the Doppler shift of backscattered electromagnetic radiation. Under clear-air conditions, scattering at these wavelengths is dominated by Bragg scattering, which arises from fluctuations in the refractive index of the atmosphere at scales corresponding to half the radar wavelength. In the lower troposphere, these refractive index variations are primarily associated with small-scale gradients in temperature and humidity. In contrast, during precipitation events Rayleigh scattering from the precipitation dominates. Observations are typically made using one vertically pointing beam and at least two additional beams tilted approximately 17° from the vertical and oriented orthogonally (i.e. separated by 90° in azimuth). These multi-beam measurements enable retrieval of the three-dimensional wind vector. The algorithm assumes that the wind field is uniform between the beams but errors in the winds can arise during localised convective precipitation when the uniformity in precipitation does not exist or there is some aliasing due to heavy rain.

During the WESCon–WOEST campaign, two RWPs were deployed at Netheravon (51.239°N, -1.778°E) and Chilbolton, providing continuous wind profiling over the study period (see Figure 1(a)). The Netheravon RWP is a mobile version of the three-panel PCL1300 boundary-layer wind profiler, manufactured by Degreane Horizon (Norton et al., 2006). The Chilbolton RWP is a non-standard five-panel PCL1300 boundary-layer wind profiler, manufactured by Degreane Horizon. The five-panel system has a four times larger vertical antenna compared to the standard system and was designed to optimise the vertical velocity measurements. Both RWPs operated at a frequency of 1290 MHz with a peak transmit power of 2.5 kW. The RWPs operated in low mode to maximise signal-to-noise ratio and achieve a high temporal resolution of under 5 minutes. In low mode, the profiler uses a Gaussian pulse of 1 μs and a gate spacing of 75 m, starting from the lowest range gate at 75 m. With 57 range gates, this provided a vertical coverage of just over 4 km depending on atmospheric conditions. Wind fields were derived from the spectral data using Degreane Horizon processing software, version 7.49(E).

https://doi.org/10.5194/egusphere-2026-4631
Preprint. Discussion started: 7 August 2026

The RWP data are averaged over 5 minutes and over 500-m in the vertical, with signal to noise ratio weighting, to match the 3D winds' vertical resolution. Considering also the data quality flag, the Netheravon RWP yields over 65,000 data points for comparison against the 3D composite from 51 days of operations. The Chilbolton RWP operated for a slightly longer period and provides 103,122 points, but 5 days' worth of data are removed due to recording zero wind throughout. However, in terms of comparisons with the 3D wind composite, these are only possible when there are sufficient hydrometeors present above the RWPs. In total, 5,387 comparisons can be made with the Netheravon RWP where at least one Doppler radar measurement is available for the composite, 2,106 of which are observed by at least three radars that cover Netheravon. These numbers are 11,959 and 998, respectively, for the Chilbolton RWP. We attribute the greater reduction at Chilbolton to the co-location of an NXPol radar and the RWP and therefore the wind profiler falls within the NXPol radar's cone of silence.

2.4 Aircraft observations

Aircraft operated on 17 IOP days during the WesCon-WOEST campaign, featuring either the Jade-One Dimona HK36, motor-glider or the UK's FAAM Airborne Laboratory BAe-146-301 Atmospheric Research Aircraft. DIMONA only operated outside cloud and is therefore not considered for verification of the multi-Doppler retrievals, which are primarily available when hydrometeors are present. During days with convective storms, FAAM would target individual storms identified by the radar operators on the ground and gather high-frequency data on temperature, humidity, wind speed, cloud microphysics, and aerosol properties (Barr et al., 2026). Winds were measured using a five-port turbulence probe on the aircraft radome (Petersen and Renfrew, 2009), with data recorded at 32 Hz; data products are described by Sproson (2024).

To verify the multi-Doppler wind estimates against the FAAM data, we focus only on periods when the aircraft penetrates convective clouds. The aircraft data are recorded with 1 s resolution, effectively a narrow line measurement, whereas the multi-Doppler estimate is at a much greater scale of 1×1 km horizontally and 500 m in the vertical. Also, the aircraft measurements are effectively instantaneous compared to the 5-minute period during which radar scans are considered to generate the multi-Doppler estimates. It is important to consider here that there is both a temporal- and spatial-scale, mismatch with the radar derived 3D wind product and the aircraft, fundamentally limiting the agreement that can be expected. The scale of observation most useful for model evaluation (and data assimilation) is likely between the two. We set a minimum transect duration of 20 s (approximately 2.5 km) for the cloud to be of sufficient size that it may be captured by the 3D composite, whereas we compare 5-s rolling averages of vertical wind. Across the 16 FAAM flying days, 28 transects were identified and will be considered for validation in Section 4.

2.5 Model simulations

In Section 3.1, we use WRF simulations to provide a background wind estimate to unfold the Doppler measurements. To support campaign planning alongside Met Office forecasts, the WRF model (Powers et al., 2017; Skamarock et al., 2019) was run in a nested configuration using two domains with horizontal grid lengths of 1.3 km and 800 m. Vertical resolution was staggered, with 51 vertical levels in total and 7 levels in the lowest 1 km AGL. The Morrison microphysics scheme was used,

https://doi.org/10.5194/egusphere-2026-4631
Preprint. Discussion started: 7 August 2026

together with the MYJ boundary-layer scheme, and the NOAH land surface model, while convection parameterisation was switched off. Model simulations were initialised using the 12 UTC NCAR GFS global analyses and forecasts.

3 Methodology

The radar processing for this study was primarily built on algorithms available in PyART (Helmus and Collis, 2016). We introduce ORIGAMI, a new technique to unfold the Doppler measurements in section 3.1, possible due to the availability of model simulations throughout the campaign period, in Section 3.1. The PyDDA multi-Doppler retrieval algorithm is covered in Section 3.3, including several additional steps developed during the processing of the WesCon-WOEST data.

3.1 Unfolding velocities: ORIGAMI

Of critical importance for the 3D wind retrieval is to de-alias the Doppler velocities derived from each radar, particularly for the NXPol radars which during WesCon-WOEST operated with a Nyquist velocity of just 12 m s^{-1}. We considered both a region based approach incorporated in PyART (Helmus and Collis, 2016) and the "UNRAVEL" technique of Louf et al. (2020). Both techniques are large improvements on use of raw data, but both have more difficulty in situations of scattered precipitation prevalent in the WesCon-WOEST data, so a more robust system was needed.

Haase and Landelius (2004) proposed the use of wind data from a “nearby sounding or from an NWP model” to simplify the unfolding, though historically the computational cost has prevented the approach from being used operationally. The prevalence of forecast simulations during the WesCon–WOEST campaign makes the approach viable for this study. When using model data, in this case the 800-m grid-length WRF forecast simulations (Section 2.5) we only require the simulated winds to within the Nyquist velocity (depends on radar, see table 1). For WesCon-WOEST, this is normally achieved, only failing in the few instances where large and intense convective cells are misplaced in the model relative to the observations.

3.2 ORIGAMI algorithm

The Observed Radar Inversion using Guided Aliasing from Model Interpretation (ORIGAMI) algorithm has been developed, unfolding each of the radar scans, done via the following procedure:

1. Model u and v winds are mapped to the polar coordinates for each individual radar and determine the radial velocities for that radar, ignoring the presence of targets (effectively assuming the entire region is surrounded by passive tracers which create no attenuation).

2. Simulated radial winds are then compared to the radar radial wind observation.

3. The integer number of folds is selected to minimise the difference between observation and model.

4. Selected number (and direction) of folds is applied for corrected velocity.

https://doi.org/10.5194/egusphere-2026-4631
Preprint. Discussion started: 7 August 2026

200 In Figure 3 we show two examples to illustrate when a region-based, or UNRAVEL, unfolding algorithms work well, but also why the model-derived unfolding is essential. When precipitation is widespread, such as in panels (a–c) UNRAVEL and ORIGAMI, the model-derived unfolding produce equivalent results. However, in the scattered situation of panels (d–f), we see that UNRAVEL struggles in certain places (for example the central shower and those to the West), where the fold may have occurred in a region between isolated cells without Doppler measurements. Because we can apply the model-derived unfolding method, regardless of whether there are targets present in between, it results in an unfolded velocity field that appears physically consistent, i.e. without gradients induced by folds. For the remainder of this study, the ORIGAMI model-derived unfolding approach is applied.

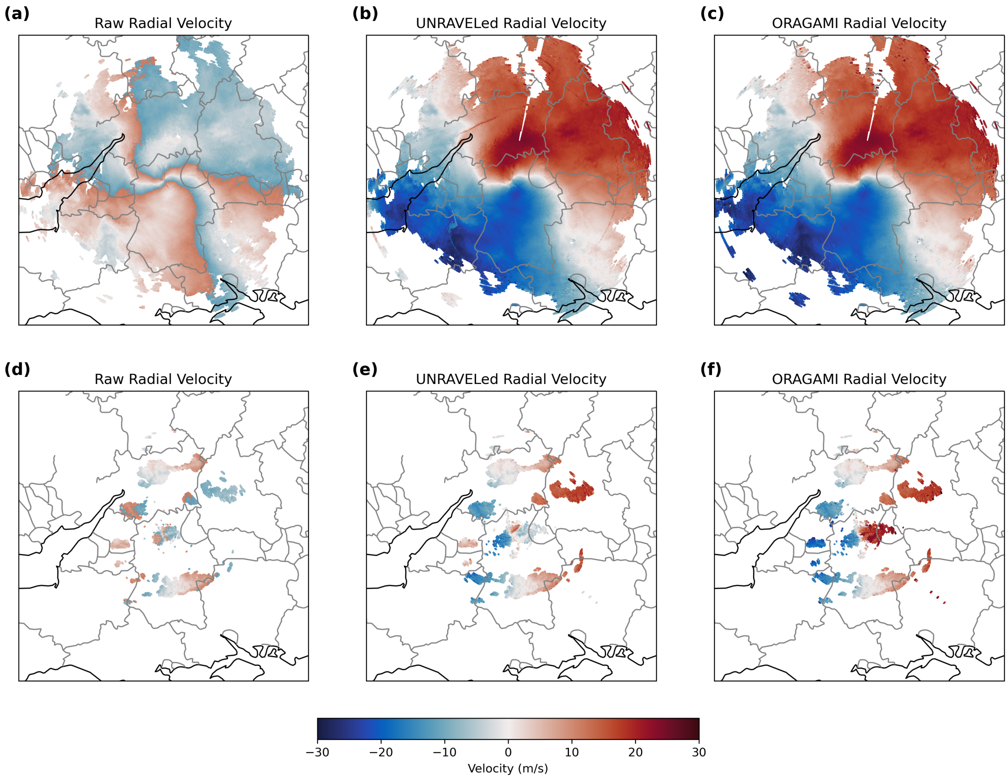

Figure 3. Radial velocities (top) during widespread precipitation on 14 July 2023 and (bottom) during scattered precipitation on 3 July 2023, as observed by the Lyneham NXPol radar. (left) Raw observed radial velocity; (centre) output from the region-based UNRAVEL algorithm; (right) output from the model-derived algorithm. The ORIGAMI system of model based unfolding is essential in scattered convection and roughly equivalent to UNRAVEL unfolding in widespread precipitation.

https://doi.org/10.5194/egusphere-2026-4631
Preprint. Discussion started: 7 August 2026

3.3 PyDDA

Derivation of the 3D wind field is done by iteration to minimise a cost function, using the PyDDA 2.4.1 framework of Jackson et al. (2020), which is an implementation of a 3D variational retrieval from Shapiro et al. (2009) and Potvin et al. (2012b). Before considering the PyDDA cost functions in Section 3.3.3, we introduce our grid configuration and the initialisation ("first guess") of the algorithm.

3.3.1 Grid configuration

The Met Office radar observations are widely used for rainfall estimation in the RadarNet rainfall product, which is generated on the UK OS grid using UK grid north as a reference. Accordingly, the raw radar data are recorded relative to UK grid north. Hence, a small but crucial correction is made to the azimuth of the Met Office radars to account for differences between true North and UK grid north (maximum change $1.13°$) prior to being used as input in PyDDA.

The next step is to regrid the radar data from polar coordinates (azimuth, elevation and range) to a structured three-dimensional Cartesian grid. The final output grid covers most of southwest England and is chosen to ensure the resolution of the Cartesian grid is not higher than the radar data that is used to generate it. The resulting region has dimensions 189 km West-East, 132 km North-South with a horizontal resolution of 1 km and a vertical resolution of 500 m (with 20 vertical levels). This grid resolution is chosen as a compromise between radar sampling across the whole grid and a desire to resolve updraft strength and sizes to constrain sub-km NWP simulation. The gridding algorithm used in Py-ART (Helmus and Collis, 2016) places the filtered polar data with weighted sphere of influence onto the Cartesian grid (Barnes, 1964; Pauley and Wu, 1990).

3.3.2 Initialisation of Wind Retrieval

PyDDA offers a range of options to initialise the 3D wind retrieval, including a sounding, NWP model output, as well as a given other profile, for example from a velocity-azimuth display (VAD) wind profile derived from a radar's Doppler measurements. The choice of initialisation profile is important for two reasons, namely (1) it enables a faster convergene to the optimised final output than if initialised with a constant or zero velocity and (2) the output defaults to the initialisation away from radar observations, so using a more realistic wind would result in a more realistic field (although such data should be used with caution).

A robust initialisation is required, which eliminates any possibility of using radiosondes, which were not frequently launched during the campaign. RWP observations are possible, but we desire to use that instrument for validation, so to maintain independence of sources, we cannot use those. Using the WRF model data would appear a reliable solution, however in a number of cases the wind profile deviated significantly from the profiles derived from other data, as for example shown in Figure 4(b). Therefore, we chose to use a VAD to initialise the retrieval, but with the following modification to improve performance.

Due to the patchy nature of convective storms, a VAD from a single radar can lead to undesirable results such as missing or uncertain information at specific heights, with winds set to 0 if no suitable VAD is available. Instead, in this unique study a composite VAD was generated which included Doppler measurements from all available radars, with the added benefit it will

https://doi.org/10.5194/egusphere-2026-4631
Preprint. Discussion started: 7 August 2026

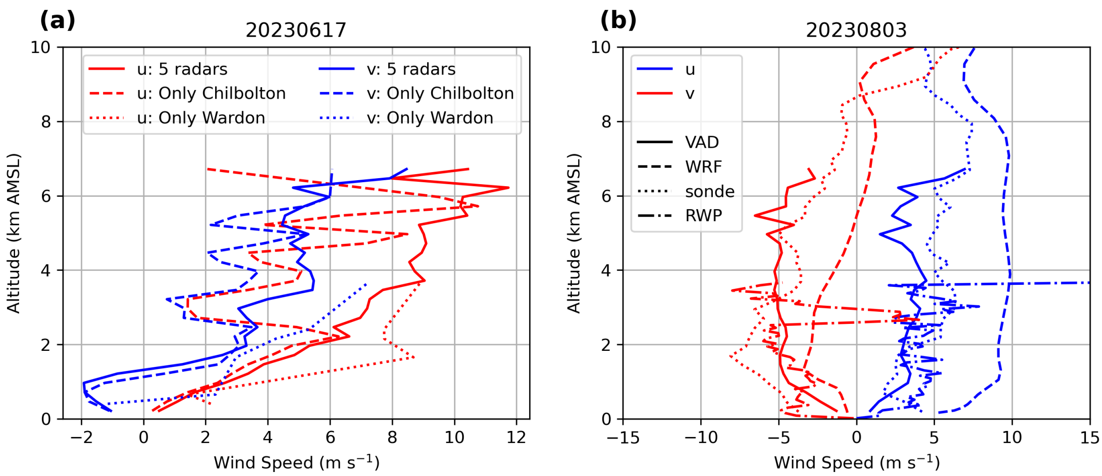

Figure 4. (a) Wind profile derived from VADs for Wardon Hill (dashed), the Chilbolton NXPol (dotted) , and all five radars (solid) for a case of scattered convection for 13:00 on June 17, 2023. (b) Mean wind profile derived from WRF, RWP, radiosonde, and VAD for 15:00 on August 3, 2023.

be a closer representation of the average across the grid. To calculate this VAD, we use the unfolded Doppler measurements from each radar, using the ORIGAMI algorithm (see section 3.2). An additional filter that removes winds smaller than ± 0.1 m s^{-1} is applied to eliminate any remaining clutter, which could significantly alter the VAD. Note that if the filter does remove genuine data (i.e. not clutter), the default in the presence of no data is 0 wind speed, which is essentially what the result of the VAD including the data would reveal. This provides data similar to the normal single radar VAD, but with potentially 5 times more observations, leading to a more complete coverage in direction and altitude. From here a sine wave is fitted at a given altitude, using all 5 radars, equally weighted. Initial winds at altitudes not covered by the VAD are set to those at the nearest available altitude, though this would be outside of the realms of radar coverage. Vertical velocities are set to 0 throughout the domain in the initial wind profile.

An example VAD wind profile for a typical case of scattered convection is shown in Figure 4(a). If only the Wardon Hill radar VAD is used, the wind profile at higher altitudes (above 3.5 km) is not known (the signal is all near the radar, so not seen at high elevations), whereas if only the Chilbolton NXPol radar is used, the profile becomes noisy at higher altitudes due to the patchy nature of precipitation for this case. The combined VAD from all five radars generates a smoother wind profile that still broadly matches that of the individual radars. This multi-radar VAD matches the radiosonde and RWP profiles significantly better than the WRF model data as exampled in Figure 4(b).

3.3.3 Cost functions

The PyDDA variational retrieval aims to minimise the cost function, J:

$$J = \Sigma_i c_i J_i \,, \tag{1}$$

https://doi.org/10.5194/egusphere-2026-4631
Preprint. Discussion started: 7 August 2026

where c_i are the weights associated with the individual cost terms J_i. The algorithm is run with a $wind_tol = 0.5$ and $max\_iterations = 25$, this potentially runs the cost function > 250 times, though has generally converges well before reaching this limit.

We are using three of the cost function terms provided in PyDDA, namely a cost related to disagreement with observed line of sight velocities, J_o; a cost for inconsistency with mass continuity, J_m; and a smoothness constraint, J_s. The vorticity constraint in PyDDA requires a single system motion, which is not straightforward to derive for the size of our domain and in the context of scattered convection, and is therefore not considered here.

$$J = c_s J_s + c_o J_o + c_m J_m \ , \tag{2}$$

Below, we briefly describe each cost function term considered and note our choices of weights, c_i. In Section 3.3.4 we introduce a a new boundary condition to PyDDA to prevent non-zero vertical winds above cloud.

Smoothness

The smoothness cost, J_s, is given by:

$$J_s = \nabla^2 \mathbf{V} \ . \tag{3}$$

The main effect of J_s is to avoid over-fitting noise and to relax the retrieval to the initial guess outside of areas with observation. We set a value of $c_s = 1$ and do not vary this. The range of weights introduced for the other terms should therefore be considered relative to our choice for c_s. In terms of the cost terms contributions, when the solution is constrained by a reasonable number of observations, the converged result will usually have the smallest remaining cost from the smoothness constraint, J_s.

Observations

The observations cost, J_o, is given by:

$$J_o = \Sigma_r \Sigma_i \left[w_i \left(V_{r,i} - \mathbf{V} \right) \right]^2 \ , \tag{4}$$

where i is each point of the Cartesian grid and r each individual radar. w_i is the radar pair combination weight calculated within PyDDA. For each point and each radar, $\mathbf{V}_{r,i}$ is the observed line of sight velocity, converted to the Cartesian coordinates of $\mathbf{V}$, the retrieved wind. The conversion of radar line-of-sight winds to Cartesian coordinates accounts for hydrometeor terminal velocities using the methodology of Mike Biggerstaff and Dan Betten (as used in for example Potvin et al., 2012a). Most grid points can be observed by several radars and potentially over half a million individual velocity values can contribute to J_o. The range of c_o we will test is 10^{-4}–10^{0}.

Mass Continuity

The mass continuity cost, J_m, is given by:

$$J_m = \nabla \cdot \mathbf{V} + w \frac{dp}{dz} \ , \tag{5}$$

https://doi.org/10.5194/egusphere-2026-4631
Preprint. Discussion started: 7 August 2026

where $\frac{dp}{dz}$ is the pressure lapse rate and we assume a standard atmosphere. Mass continuity is calculated using the grid spacing and J_m is therefore orders of magnitude smaller than J_o, so the range of c_m we will test is 64–16384.

3.3.4 Capping at Cloud-Top

We have introduced a rule to PyDDA designed to solve a specific problem. With the system as described to this point, we resolve vertical wind "flares" above cloud - stretched from vertical winds detected in cloud, reaching from in cloud to the defined grid top. While caution should always be used where radar observations are not present, it is certainly preferred to have a more realistic field if possible. The choice of grid top is made for radar coverage and a likely approximate tropopause level, however, we can adjust the effective lid boundary condition to be above the cloud. PyDDA's mass continuity function introduces the option ("$upper\_bc$" within the PyDDA code) for the upper boundary condition as permeable or impermeable via amendments to the gradient of the cost function. We have implemented a 3rd option to the $upper\_bc$ parameter, implementing a choice for the atmosphere to be impermeable above the highest detected cloud, via the same methodology, spread down to the cloud top.

3.3.5 Selection of and Sensitivity to Weights

In Figure 5 we show the retrieval for a typical convective cell observed during the field campaign for various combinations of weights for mass continuity and observations, in all cases the smoothing terms all have weighting of 1. This figure shows that with high observation and low mass weights (top-right) there are extreme transitions and high vertical velocities that are unlikely to be realistic. The reverse, low observation and high mass weights (bottom left) result in a very smoothed out field, as the observations don't have the ability to markedly change the local flow from the initialisation. A subset of combinations of c_m (256–16384) and c_o (10^{-4}–10^{-1}) will be evaluated against RWP and aircraft observations in Section 4.1 and Section 4.2.

3.3.6 Output

The default configuration of PyDDA applies a low-pass filter to the output after minimising the cost function. Because we are interested in spatial scales close to our grid resolution we have chosen our grid configurations so that our observations match or exceed this resolution and have therefore switched off the post-processing filter. The final output is stored as a NetCDF-4 file containing the three-dimensional grid of u, v and w (North given by true north), with one file for every scan cycle, i.e. every 10 minutes. Each file also includes information at each grid point of (1) the final cost functions (each of J_s, J_o and J_m), (2) a count of the number of radar observations used, and (3) the median of radar reflectivity. Also included are the initialisation profile as calculated by VAD (section 3.3.2) and appropriate metadata. The files are available on the CEDA archive, with DOI: **DOI for data**. A file is available every 10 minutes for the WesCon-WOEST campaign, sorted by date, with filesnames following the convention: **"WOEST_windgrid_1000m_YYYYMMDD_HHMM_v1.0.nc"**.

https://doi.org/10.5194/egusphere-2026-4631
Preprint. Discussion started: 7 August 2026

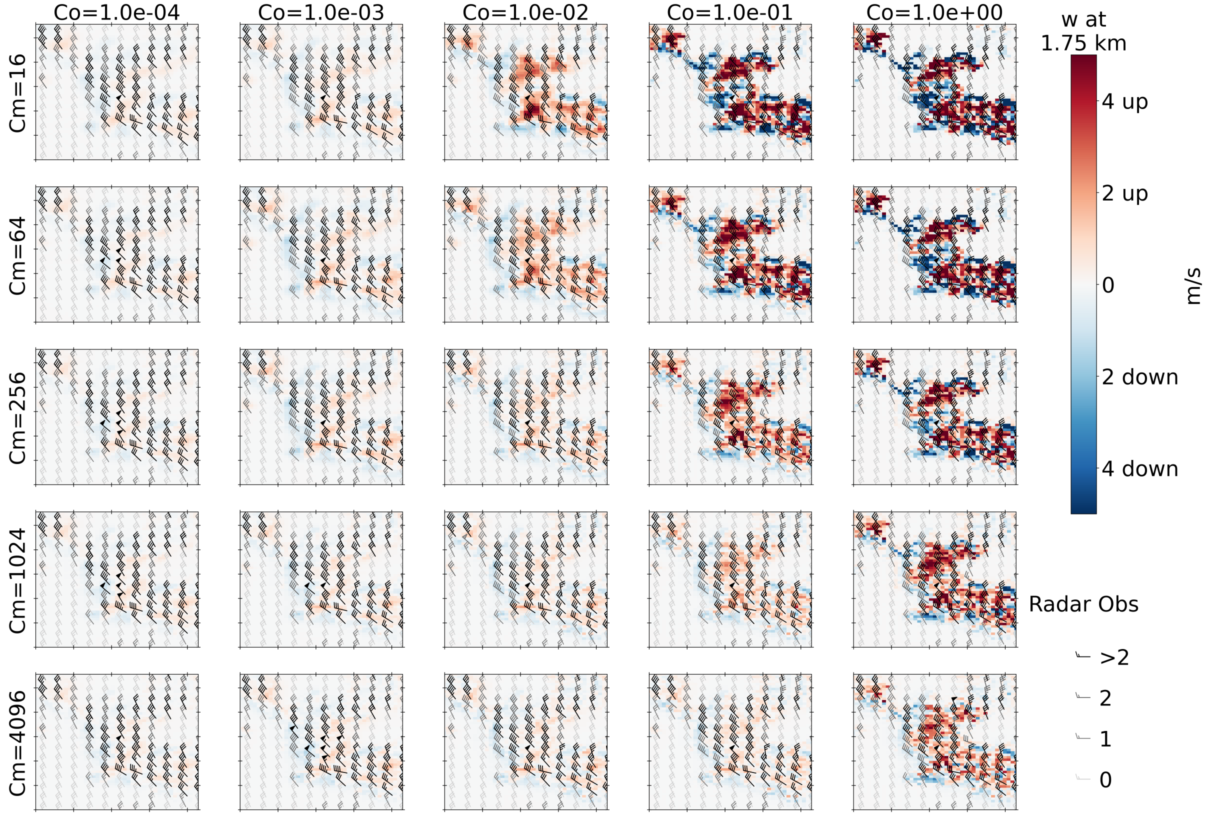

Figure 5. Sensitivity of the PyDDA-retrieved winds to choice of weights, with $c_s = 1$, c_o increasing by a factor 10 from left to right, and c_m increasing by a factor 2 from top to bottom. Individual panels show the retrieval for the same convective cell with horizontal wind barbs and w (in colour) at 1.75 km. Grey shading of the horizontal wind barbs indicates the number of radars observing the location. Tick marks are separated by 10 km.

4 Validation

We validate the PyDDA retrievals against two data sets available for the WesCon-WOEST campaign, namely, the radar wind profilers (RWP) and the FAAM aircraft measurements. For both validations, we compare the output of the full ORIGAMI and enhanced PyDDA retrieval, as described in section 3, using cost function weightings as discussed in that section, $c_s = 1.0$, $c_m = 4096$ and $c_o = 0.01$ (the default setup). Section 5 will examine the sensitivity to these weights and explain their selection as the choice for this work and dataset.

4.1 Radar Wind Profiler Comparison

The radar wind profilers (RWP) used in this work are described in section 2.3 and provide u and v. RWP, at this wavelength, vertical motion is dominated by the fall speed of Rayleigh scattering precipitation, which could not be corrected for given the

https://doi.org/10.5194/egusphere-2026-4631
Preprint. Discussion started: 7 August 2026

data recorded. It was not possible to separate the secondary Bragg scattered air motion signal. As a result we only consider the horizontal winds for this verification.

Figure 6 provides a comparison between the PyDDA retrieval and the Netheravon RWP for a single day. The day was selected because of the significant wind shift, shortly before 15:00, which is particularly visible in the v component of the wind (bottom panels). The PyDDA retrieval clearly captures this wind shift both in u and in v, although there are some obvious differences between the two datasets. The RWP measurements are recorded at higher vertical resolution and temporal resolution compared to the PyDDA retrieval, we coarsen the former to the same vertical grid and smoothen it temporally. For our verification, only grid points where the RWP records sufficient signal to noise ratio (SNR) and at least one radar measurement is available ($N_{radar} > 0$, top-right panel) were used.

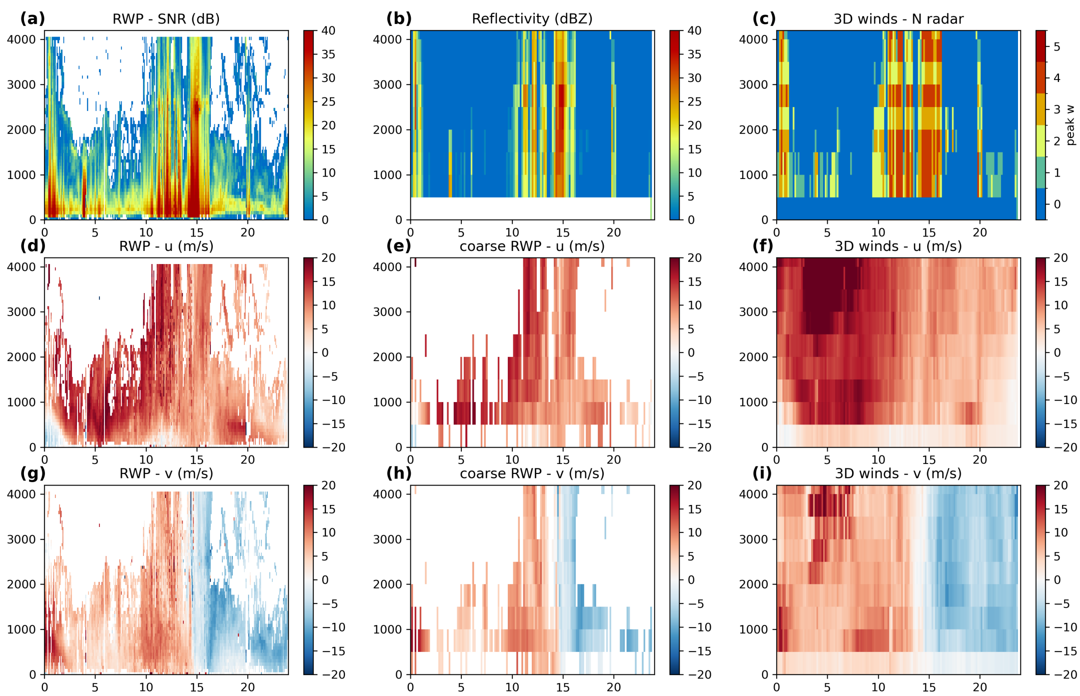

Figure 6. Comparison between RWP and the PyDDA retrieval on August 2nd, 2023 at Netheravon, showing the u (middle row) and v (bottom row) wind components. (a) RWP signal to noise ratio, (b) radar reflectivity (median of the 5 radars) and (c) the number of radars providing Doppler velocities. The u component of wind is shown (d) on native RWP resolution, then (e) degraded to the 3D winds grid and (f) 3D winds derived value. Panels (g), (h) and (i) repeat those with the v wind compnent.

https://doi.org/10.5194/egusphere-2026-4631
Preprint. Discussion started: 7 August 2026

In Figure 7, we compare u and v PyDDA retrievals from the entire WesCon-WOEST campaign against the Netheravon and Chilbolton RWP data. The RWP data have been coarsened as illustrated in Figure 6. The data have been categorised by the number of radars available for each retrieval (which may vary due to radar availability and data quality).

The verification is carried out separately for retrievals above and below 2 km altitude. Evident in Figure 6 is that the 3D wind retrieval has much lower wind speeds closer to the surface, compared to the RWP observations. This may be due to a lack of observations, as the radar beam height increases with distance from the radar, but also due to the smoothness constraint and mass flux, which expects $w = 0$ m s^{-1} at the surface.

In the scatter plots in figure 7 there is very strong correlations, above 0.9, for both u and v, and root-mean-square errors are typically below 3 m s^{-1}, with a reduction to below 2.4 m s^{-1} when 3 or more radars are observing the area. However, a bias is noticeable in u, above 2 km altitude, which is not reduced by addition of more radars observing. The bias in v is smaller, but reverses sign with the addition of more radar observations. Given the results suggest different bias in wind components, we also consider the horizontal speed. The verification metrics for horizontal wind speed are similar to those for u and v.

While the 3D wind retrieval appears reliable, the bias in u particularly above 2 km, even when multiple radars are available, must be considered when interpreting wind patterns, as for instance as shown in section 6.

Overall, the comparison shows good performance with approximately 2.4 m s^{-1} root mean square errors when viewed by 3 or more radars. Fundamental features of the design and observational geometry are the likely cause of the reduced observation of low wind speeds, though note that addition of local observations rapidly improves the statistics.

4.2 FAAM

To introduce the comparison against FAAM aircraft measurements, we first provide a case study example. Figure 8 shows the aircraft vertical velocity, w, measurements for one of the longest transects of the campaign, where the aircraft remained within cloud over a distance of approximately 20 km sampling a number of updrafts of a range of strengths and horizontal scales. Alongside the transect we show the PyDDA retrievals for the location of the aircraft, choosing the nearest available time and interpolating in space, with colour-coding indicating the number of radars observing the grid point.

The single transect includes a few periods where the PyDDA retrieval compares well, e.g. between 11.9 and 12.1 hrs, and broadly the distribution of w appears reasonable, though without the peaks visible from the aircraft. However, a few major discrepancies are also evident. At approximately 12.55 hrs (decimal hours, with fractional values representing fractions of an hour), an weak updraft with 4 radar coverage appears in the PyDDA retrieval but with little vertical motion experienced by the aircraft. On the other hand, a narrow peak is detected by the aircraft at about 12.6 hrs, exceeding 5 m s^{-1}, but the PyDDA retrieval remains below 1 m s^{-1}. Both instances could be due to temporal mismatch and/or spatial mismatch. We consider 9 s averages in the aircraft data, approximately 1000 m horizontal distance, essentially a line through 3D space, while the wind retrieval considers the motion over a 0.5 km^3 volume.

The retrieval also considers observations gathered over a 5-minute period, which may further smooth possibly transient features that the aircraft could experience. As a result, the representivity is not expected to be perfect.

https://doi.org/10.5194/egusphere-2026-4631
Preprint. Discussion started: 7 August 2026

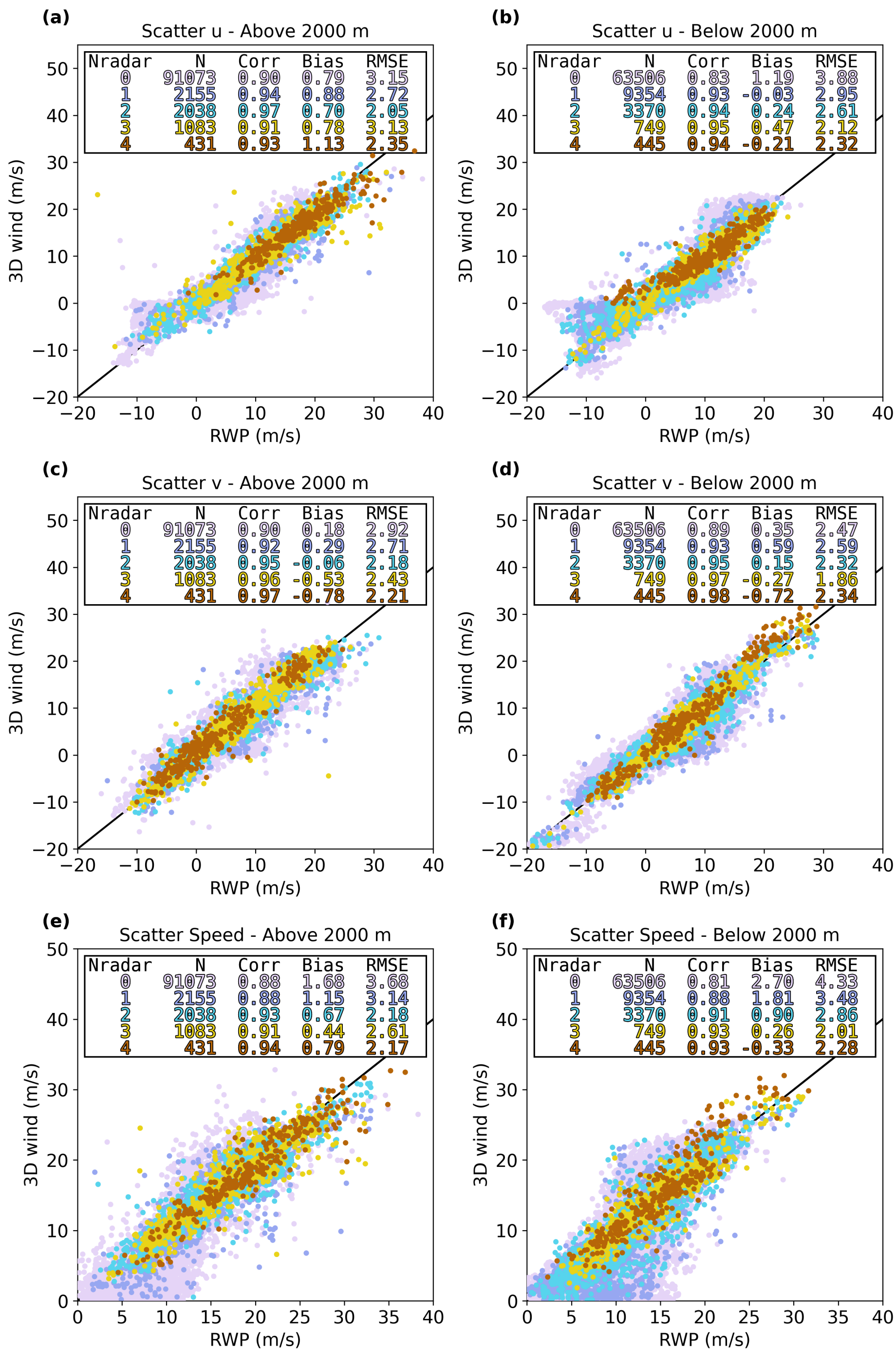

Figure 7. Comparison of PyDDA retrievals against the RWPs at Netheravon and Chilbolton. The left plots (a,c,e) show the matches with altitudes above 2 km, the right plots (b,d,f) below 2 km. Top plots (a) and (b) are for the u component of wind, middle plots (c) and (d) the v component of wind and wind speed the lower plots (e) and (f). Colours indicate the number of Doppler radar observations accepted for the variational scheme. Each panel includes statistics based on the number of observing radars.

https://doi.org/10.5194/egusphere-2026-4631
Preprint. Discussion started: 7 August 2026

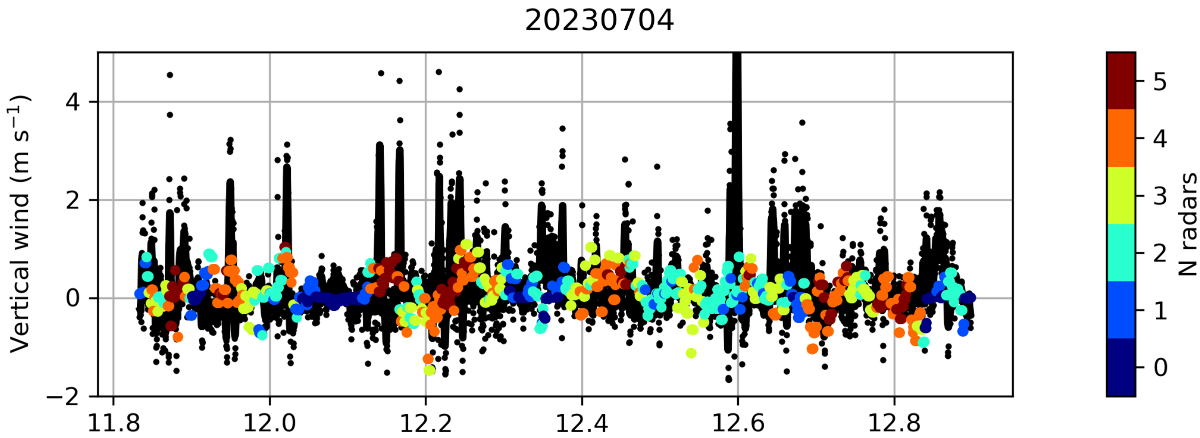

Figure 8. Comparison of in-cloud PyDDA retrievals against aircraft measurement for a transect of the FAAM flight on 4th July 2023. Black dots show the 1 s resolution vertical wind recorded by the aircraft, with a black line a running 9 s mean (to have approximate 1 km horizontal scale). Coloured points are the 3D wind field interpolated to the aircraft time and location, with colour determining the number of radars available for that wind field.

Statistical View

Given the issues of representivity between the essentially point measurement of the aircraft, and the volume of the retrieval, we now consider a statistical approach to verification against the FAAM measurements. Across the 28 transects with suitably long cloud observations, we assume that the population of updrafts sampled by the aircraft and the PyDDA retrieval (subsetted along the aircraft transects) will be of similar size and strength, even if they are not matched exactly in space and time.

Figure 9 shows the histograms of w from the FAAM transects and nearest PyDDA retrievals above and below 2 km altitude. The PyDDA retrieval clearly underestimates stronger updrafts and downdrafts, particularly above 2 km altitude. Below 2 km altitude, the PyDDA retrieval still underestimates updrafts, although it appears to better capture downdrafts, likely because are generally observed to be weaker than higher up. Although this analysis suggests that the PyDDA retrieval does not perform well in terms of direct w comparisons, and has reduced scale of updrafts, we emphasise that FAAM preferentially sampled relatively smaller and weaker convective storms, which may be more difficult to capture in our PyDDA grid configuration.

The upcoming discussion section, 7, will include a further vertical wind comparison between instruments (high resolution RHIs), which has further limitations but a useful complement to the FAAM aircraft comparison presented here.

5 Sensitivity Tests

An important consideration already mentioned is the choice of weights for the cost functions described in section 3.3.3. We consider weights to gain the best setup for accurate and useful results. In section 3.3.5 the combinations of c_m and c_o to be considered were reduced to four possibilities of each, leading to 16 combinations. These 16 combinations are run for 5

https://doi.org/10.5194/egusphere-2026-4631
Preprint. Discussion started: 7 August 2026

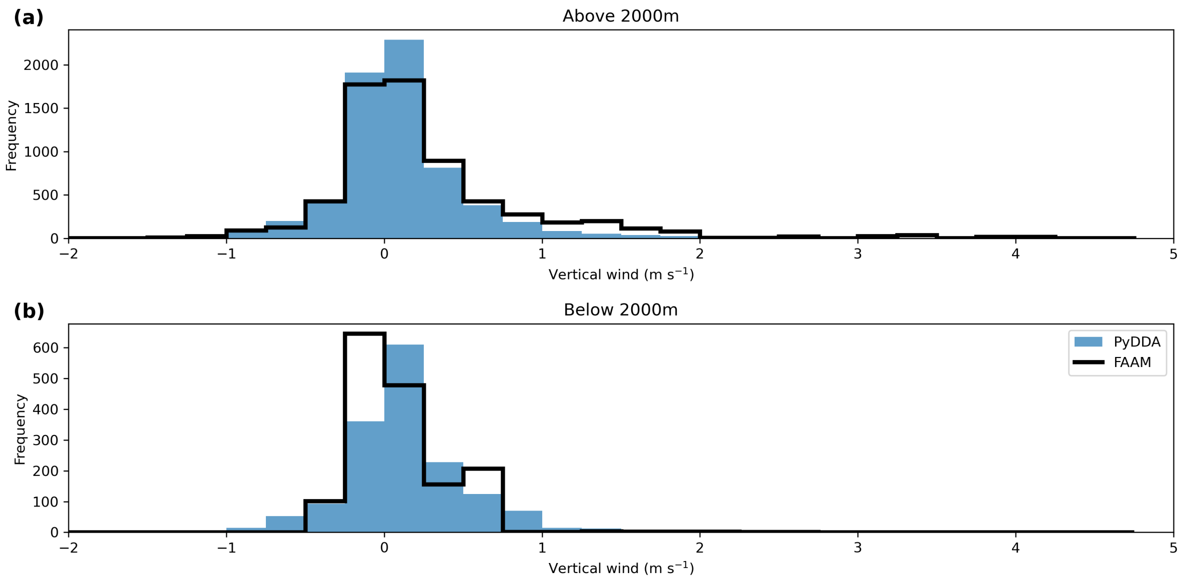

Figure 9. Histograms of vertical winds (positive upward) from FAAM transects (black) and PyDDA retrievals (blue) for the nearest time stamp and spatially interpolated to the aircraft location. Comparison is separate between measurements above 2 km altitude (a) and below (b).

complete days, selected to be ones with many matched RWP measurements to maintain good sampling statistics while limiting the required runs and data for many experiments.

Wind Profiler

Statistics can be made for each experiment matching those in figure 7, for the 5 days in the sensitivity study. For our selection we are most concerned with accuracy within convective features, so we limit our consideration to areas where 3 or more radars observe the pixel and we continue the separation of above (total of 485 matched in time and space pixels) and below 2 km (total of 440 matched in time and space pixels) due to possible differences near the ground. For each measure of correlation, bias and root mean square error, each of u, v and horizontal speed, as well as heights, we calculate the experiment with the best value and determine via bootstrapping which other experiments results are not significantly worse (at the 95% level), displayed in figure 10.

The results show no consensus of best settings from the tests, but also while the significance test can differentiate values, the measures of match (correlation and RMSE) show little variation, suggesting that the sensitivity to weights is not significantly problematic. The selected configuration (marked by a black circle) is picked either to be beside the best ($c_m = 4096$ and $c_o = 0.01$), or not statistically significantly different from the best for the measures considered. The only exception to these

https://doi.org/10.5194/egusphere-2026-4631
Preprint. Discussion started: 7 August 2026

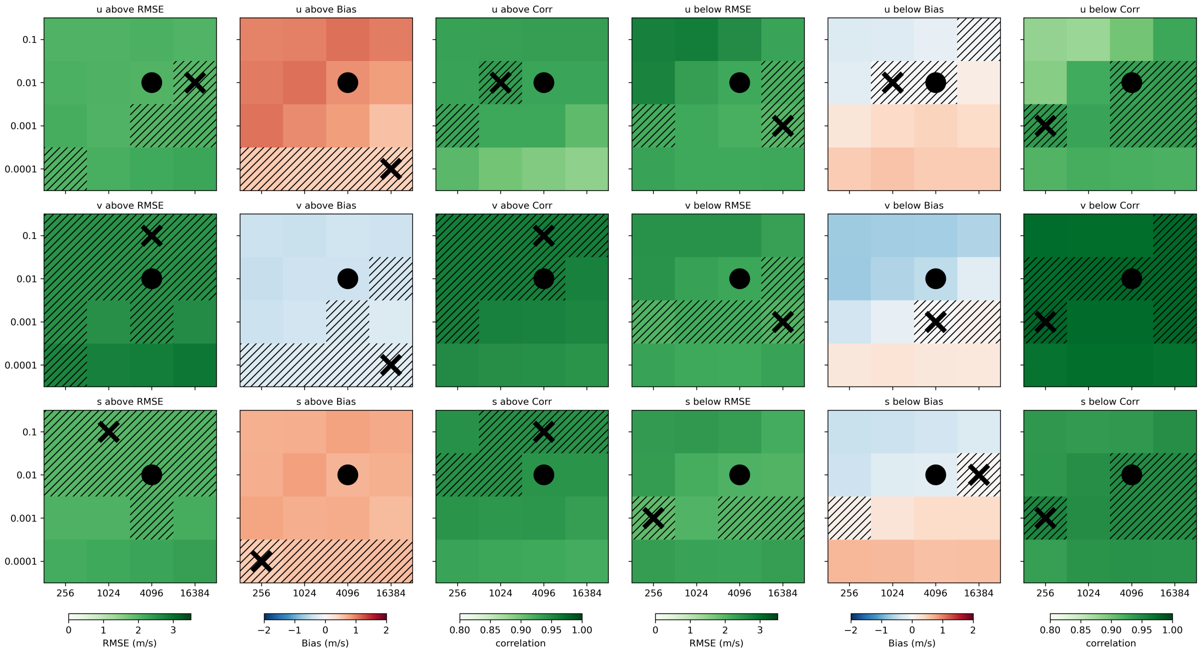

Figure 10. Chart demonstrating the significance tests. Each chart shows the 16 experiments arranged by c_m and c_o for a different test. Each column of plots shows a measure and altitude, with rows being u (top), v (centre) and speed (bottom). In each case the best statistic marked by a black cross, with hashes to designate experiments not statistically significantly different to the best at the 95% level. The black circle shows the chosen settings.

criteria is the above 2 km altitude bias. The decision to ignore bias here is because addition of more radar data worsens the bias, suggesting this will not be a result of weighting choices.

FAAM flights

For the 16 experiments there are 3 cloud passes by the FAAM aircraft to confirm suitable weighting selection and that the sensitivity is not damaging to the output, assessed by the histograms as seen in figure 9. These histograms (not shown) demonstrate that $c_o = 10^{-4}$ fails to generate significant vertical winds (observations cannot adequately overcome the initialisation). Setting c_m to 16384 allows the greater vertical winds, but retains an excess of close to zero vertical wind, a low c_m of 256 results in an excessively flat histogram, without enough low w. The histograms around the middle of the tested weights are similar and the closest matches to the FAAM aircraft data, confirming what we determined from the wind profiler, that $c_m = 4096$ and $c_o = 0.01$ creates a good retrieval without excessive sensitivity to the weights. That setting is used for the full WesCON-WOEST period, presented in the validation of section 4, this section has confirmed this selection of c_m and c_o and demonstrated there is not extreme sensittivity to the selection.

https://doi.org/10.5194/egusphere-2026-4631
Preprint. Discussion started: 7 August 2026

6 Case study examples

In this Section, we demonstrate two of the desirable qualities of the ORIGAMI and enhanced PyDDA retrieval to illustrate the types of analysis that may be possible with these data for the WesCon-WOEST campaign. Both examples use $c_m = 4096$ and $c_o = 0.01$ as determined from our best selection.

Figure 11 shows consecutive wind retrievals of a typical persistent convective storm observed during the WesCon-WOEST campaign, observed on August 3rd, 2023. For this case, the relative size, strength, and the storm relative position of the downdraft and updraft is consistent between each 10-minute wind retrieval. There is also a clear succession and evolution of individual updrafts that can be identified in this storm, which is typical behaviour seen throughout the campaign. We can observe updrafts located on the leading edge/North side of the storm, with a broad downdraft region trailing. This example has the highest reflectivity collocated with the updrafts, although we note from other cases that this is not consistent behaviour, where the updrafts are frequently ahead of the strongest reflectivities.

Figure 12 shows E-W and N-S cross-section of one of the strongest updrafts retrieved from the whole campaign, selected to show what is possible. This storm was broadly eastward propagating and we see most variability in the winds in the E-W direction, including two updraft cores about 7 km apart and a downdraft aloft further upstream, possibly related to a dissipating cell. The updraft at 2.55 °W is trailed by a vertically extending downdraft. In the N-S direction, there is limited information in horizontal wind component, but the reflectivity indicates regular spacing of cells at 10 km apart. In the vertical the peak w tends to be situated above the highest reflectivity values, but the updraft is seen to be sloping to the North-side (left of system motion).

Both the temporal consistency and the clear spatial information regarding the updrafts and downdrafts are new and crucial information to evaluate NWP simulations. In the next Section, we evaluate the wind retrievals against other estimates available from the WesCon-WOEST campaign.

7 Discussion

7.1 Spatial Scales of Updrafts

The PyDDA retrieval provides wind estimates with physically plausible estimates of updraft strength and sizes, suitable for comparison to sub-km NWP simulation for particular convective situations, as illustrated with the case studies in Section 6. The comparison of u and v against RWP measurements shows a strong correlation and low RMSE, although a slight bias is found particularly for u estimates above 2 km altitude. The comparison of w against FAAM measurements indicate a general underestimate of w in both updrafts and downdrafts, although this may be partly affected by the aircraft preferentially sampling weaker and smaller cells that our PyDDA grid configuration smooths.

The WesCon-WOEST campaign features a third independent dataset from CAMRa, introduced in Section 2.2.2, that we now briefly consider for qualitative comparison. The CAMRa RHIs are recorded at 75-m range gates and 0.28 ° beam width and hence provide a separate comparison of horizontal scales comparable to the FAAM measurements, but w is not measured

https://doi.org/10.5194/egusphere-2026-4631
Preprint. Discussion started: 7 August 2026

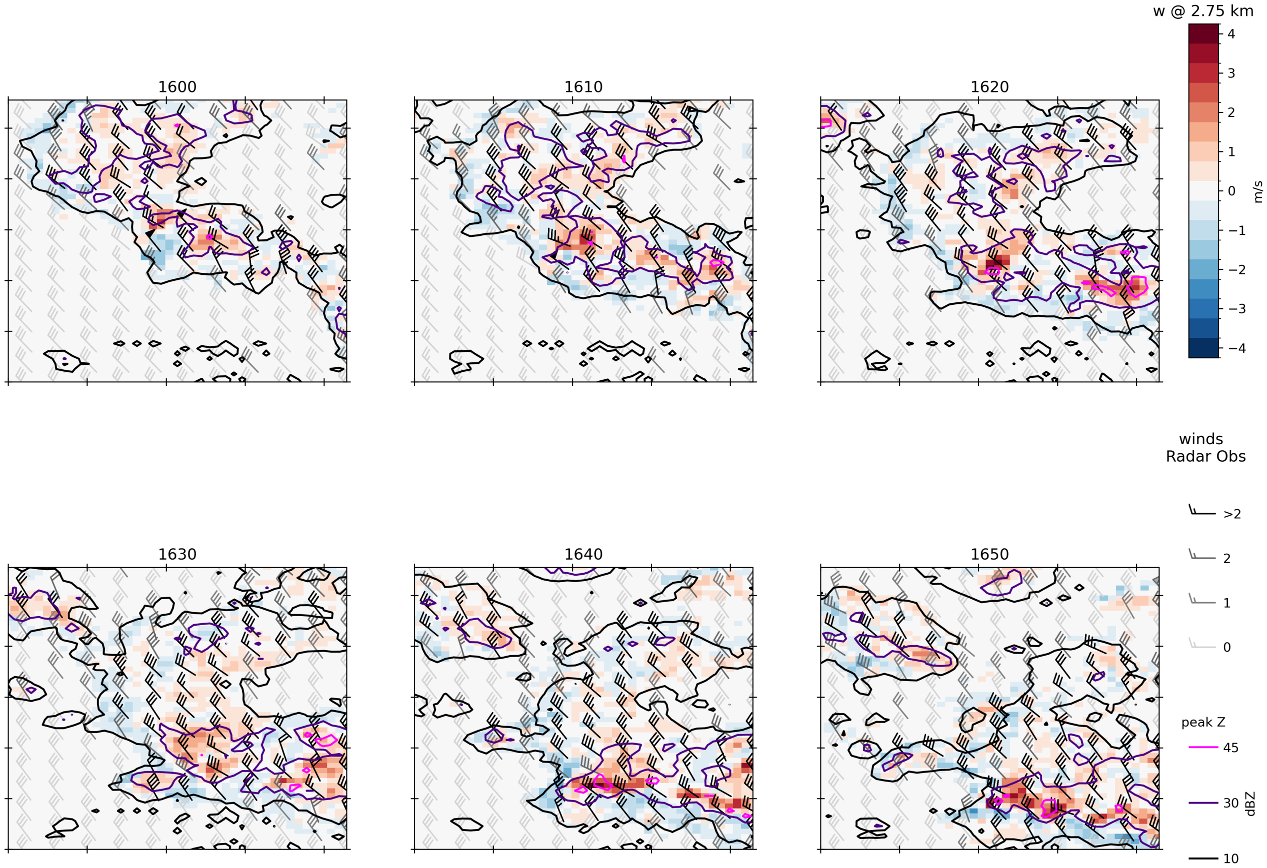

Figure 11. Example of six consecutive 3D wind retrievals of a storm observed on 3 August, 2023, showing w (colour) and horizontal wind (barbs) at 2.75 km altitude. The grey shading of the barbs indicates the number of radars providing Doppler measurements for that grid point. Purple contours show the maximum reflectivity in the vertical column. Tick marks are provided every 10 km.

https://doi.org/10.5194/egusphere-2026-4631
Preprint. Discussion started: 7 August 2026

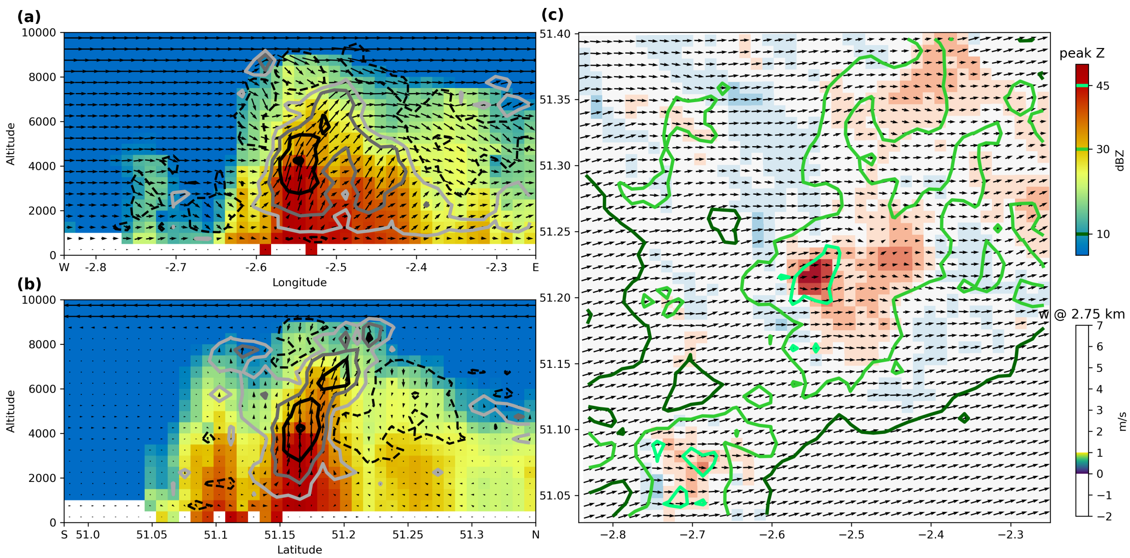

Figure 12. Case example of one of the strongest vertical motions retrieved, for a storm observed at 13:30 on 2nd August 2023. E-W cross section (a) and N-S cross section (b) showing median radar reflectivity in colour with contours of vertical wind speeds and quivers to demonstrate direction of flow parallel to the viewing pane. Panel (c) shows the planar view, with the 4.25 km altitude (where the highest occurs) vertical wind speeds in colour, quivers for the u and v wind components at that altitude and green contours of highest reflectivity in the column.

and instead estimated from Nicol et al. (2015), and hence is not a "pure truth". The Nicol et al. (2015) retrieval is purely based on the mass flux constraint and assumes zero divergence across the range-height plane of view. Hence, it will underestimate up- and downdrafts and is only used here to demonstrate the potential underestimation in the 3D wind retrieval's peak vertical winds due to resolution.

In Figure 13, we show two examples of the w estimated from a CAMRa RHI scan and the equivalent pseudo-RHI obtained from the PyDDA retrieval. (a) and (b) show a convective cell with updrafts and downdrafts that are approximately 1 km wide in the CAMRa RHI, which can be matched to a broader updraft and downdraft in the pseudo-RHI derived from the PyDDA retrieval. It appears that the higher resolution of the CAMRa data may be largely averaged by the coarse resolution of the 3D wind retrieval - resulting a loss of detail. Panels (c) and (d) show a convective cell with greater horizontal variability in w in the Nicol et al. (2015) estimates from the CAMRa RHI, but that are matched to a broadly rising feature in the pseudo-RHI. The two CAMRa scans are both close to a 10-minute time stamp, although we note that the PyDDA retrieval uses data from a 5-minute window, so some spatio-temporal smoothing will still take place. Nevertheless, this qualitative comparison further illustrates that PyDDA shows similar overall patterns, but is unable to capture weaker and narrower updrafts, due to its resolution.

https://doi.org/10.5194/egusphere-2026-4631
Preprint. Discussion started: 7 August 2026

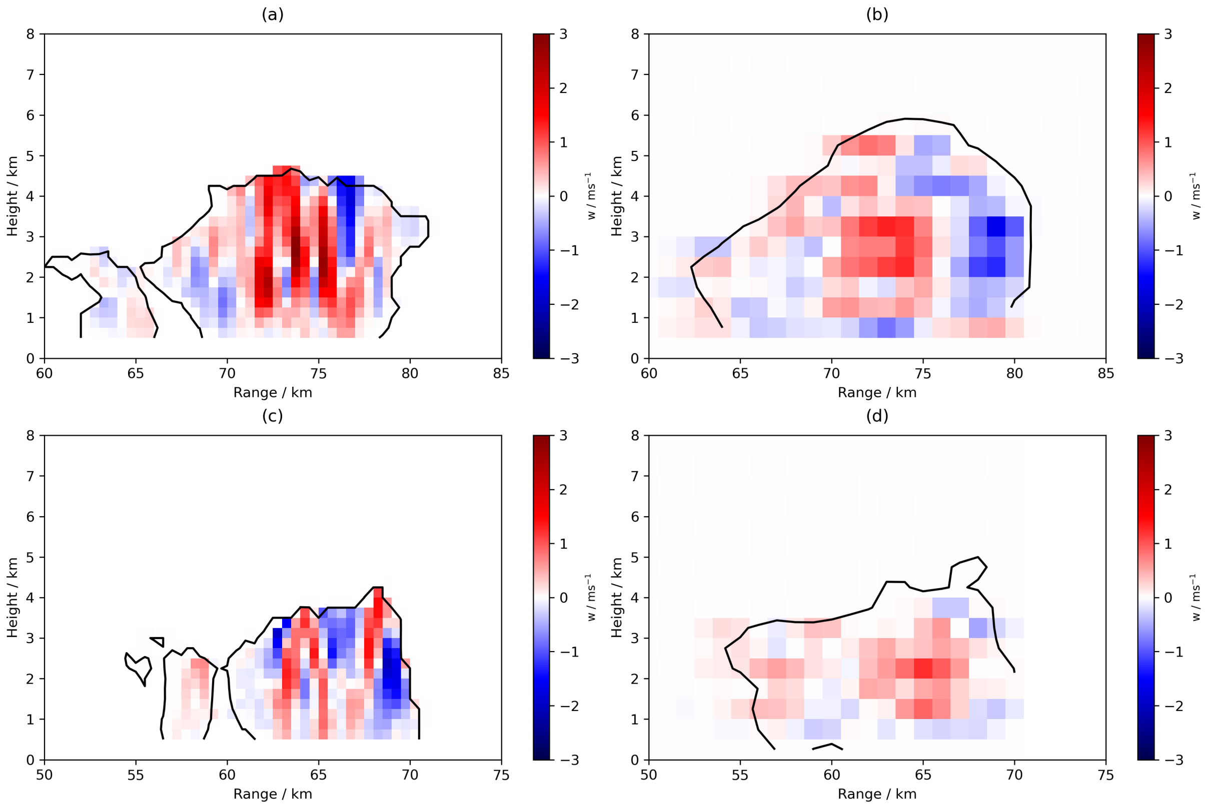

Figure 13. Vertical motion estimated using the Nicol et al. (2015) methodology for two CAMRa RHI scans (a) and (c) with the PyDDA retrieval sampled for the equivalent pseudo-RHIs in (b) and (d). The black line shows a 5dBZ contour to signify the location of cloud. Both cases occur on 3 August, 2023, the (a) and (b) at 1310Z and (c) and (d) at 1500Z.

7.2 Low Altitude Retrieval Limitations

Below 2 km altitude the retrieval accuracy shows some signs of decrease, particularly where less observations are present. This likely reflects a combination of methodological and observational limitations. The imposed $w = 0$ boundary condition at the surface, together with mass continuity and smoothing constraints, act to relax the solution toward zero vertical velocity — similar to the behaviour observed above cloud prior to the inclusion of the cloud top boundary condition (section 3.3.4). In addition, the radar viewing geometry contributes to this: at low altitudes, beams are typically at shallow elevation angles and are less frequently sampled by multiple radars. As a result, a reduction in retrieval quality near the surface is likely unavoidable.

A potential step to limiting the bias seen near the surface would be to increase the grid resolution. While this would not help with the observational limitations, it could act to reduce the smoothing effect of the mass and smoothing constraints. Limited tests have been run at higher resolutions that appear stable; future work will be needed to consider if this solution genuinely reduces the errors at lower altitudes.

https://doi.org/10.5194/egusphere-2026-4631
Preprint. Discussion started: 7 August 2026

8 Conclusions

This paper has presented the first multi-Doppler radar derived wind data set for the UK. Radar observations made during the WesCon-WOEST campaign in 2023 by five C- and X-band radars with a range of scan strategies contributed to the final 3D wind product.

The 3D winds dataset

The wind dataset complements the 3D radar reflectivity composite (Scovell and Al-Sakka, 2016) and has the same 1-km horizontal resolution and 500-m vertical resolution. The data is available for use on the CEDA data archive.

Methodological Advances

Doppler velocities were de-aliased using a new algorithm, ORIGAMI, which assumes NWP model winds as the true wind, and the radar winds are unfolded to reach the closest match within the Nyquist interval. This approach provides a more reliable result compared to region-based de-aliasing techniques, particularly in scattered precipitation. The reliability of this approach for unfolding scattered echo cases means that the authors recommend running WRF (or similar numerical models) alongside Doppler radars, noting the accuracy needed for useful unfolding is not difficult to achieve.

Winds are retrieved using PyDDA, minimising a cost function considering mass continuity, smoothness, and difference with observations. A new constraint is introduced to reduce spurious w above cloud, which otherwise persist to the top of the domain. Several combinations of weights for the different cost functions are considered and evaluated against radar wind profiler and aircraft measurements and the best compromise costs selected for the final dataset.

Performance

Verification against two radar wind profilers situated within the grid indicates that the PyDDA algorithm performs well, with RMSE typically below $4\ \mathrm{m\,s^{-1}}$, and correlation above 0.87 - both values significantly better when 3 or more radars observe the voxel, as is common with cloud. Below 2 km altitude, the bias in the retrieval is about $1\ \mathrm{m\,s^{-1}}$, possibly due to the constraint to have $w = 0\ \mathrm{m\,s^{-1}}$ at the surface and the secondary impact this has on the smoothness constraint. Verification of w against aircraft measurements suggests an underestimate of peak w in both updrafts and downdrafts, although this may be due to the aircraft preferentially sampling smaller and weaker cells. A qualitative comparison against w estimated in CAMRa RHIs further emphasises the challenges the multi-Doppler radar retrieval will have with weaker cells and updraft sizes near the grid scale.

The CAMRa dataset presents an opportunity for further validation and study of convective storm dynamics. Firstly, CAMRa sampled updraft cores every two minutes with sets of four RHI scans, with individual scans slightly separated in azimuth. Compositing of these four RHIs might enable a better and fairer comparison in terms of spatiotemporal matching with the PyDDA retrieval. Analysis of consecutive sets of CAMRa RHI scans may further strengthen analysis of the spatiotemporal

https://doi.org/10.5194/egusphere-2026-4631
Preprint. Discussion started: 7 August 2026

consistency of updrafts and downdrafts identified in the 3D wind composite. Secondly, the 3D wind retrieval could provide an estimate of divergence across the CAMRa RHI plane-of-view and hence a better constraint for the Nicol et al. (2015) retrieval.

Context for Interpretation

The results show great promise to use the PyDDA-retrieved 3D wind data set for NWP model evaluation. The wind data show good temporal consistency as well as spatial coherence in updraft and downdraft locations. Caution will need to be applied when considering winds below 2 km altitude or evaluating updraft and downdraft features less than about 2 km in horizontal scale.

Overall, the full 3D wind retrieval presented provides a unique dataset. The product is valuable for assessing storm structure, temporal consistency, other observation systems and NWP evaluation. In the UK and for the WesCon-WOEST campaign (Barr et al., 2026), joint analysis with other observations, including further aircraft measurements, turbulence estimates, and surface observations should shed new light on the evolution and controls on small-scale convective storms.

Data availability. The files are available on the CEDA archive, with DOI: **DOI to be confirmed**.

Author contributions. RJT contributed to data curation, software, formal analysis, visualization, validation, investigation, methodology, conceptualization, and writing – original draft and writing – review & editing. THMS contributed to conceptualization, methodology, supervision, writing – review & editing, project administration, and funding acquisition. CHBL contributed to software, formal analysis, visualization, validation, and writing – review & editing. RJ contributed to software and writing – review & editing. CDW contributed to conceptualization, methodology and writing – review & editing. SC contributed to conceptualization, software and writing – review & editing. LR contributed to data curation, software, and writing – review & editing. TD contributed to data curation and writing – review & editing. EGN contributed to data curation, software, and writing – review & editing. PAB contributed to data curation, project administration, and writing – review & editing. RRN3 contributed to conceptualization, supervision, writing – review & editing, project administration, and funding acquisition.

Competing interests. The authors declare no conflict of interest. The funders had no role in the design of the study; in the collection, analyses, or interpretation of data; in the writing of the manuscript, or in the decision to publish the results.

Acknowledgements. This research was primarily supported by the NERC WOEST project grant NE/X018539/1. CHBL was funded by the NERC CLOUDYTIME project grant NE/X018547/1. RJ and SC were funded by the Observationally Based Resource Assessment and Coupled Models project of the U.S. Department of Energy Critical Materials and Energy Innovation / Integrated Energy Systems Office under contract DE-AC02-06CH11357. The authors would like to acknowledge the Atmospheric Measurement and Observation Facility (AMOF), a Natural Environment Research Council (UKRI-NERC) funded facility (NE/Y005376/1), for providing the data and operation of NXPol

https://doi.org/10.5194/egusphere-2026-4631
Preprint. Discussion started: 7 August 2026

radars and radar wind profiler. Airborne data was obtained using the FAAM Airborne Laboratory BAe-146-301 Atmospheric Research Aircraft [ARA], operated by Airtask Ltd, managed by the National Centre for Atmospheric Science, leased through University of Leeds, and owned by UK Research and Innovation and the Natural Environment Research Council (NE/T014849/1). WRF data used in this study was run and provided by the FORCE group, based in the University of Leeds, Ralph Burton, James Groves, Laurents Marker and Alex Roberts.

https://doi.org/10.5194/egusphere-2026-4631
Preprint. Discussion started: 7 August 2026

References

Barnes, S. L.: A technique for maximizing details in numerical weather map analysis, Journal of Applied Meteorology (1962-1982), pp. 396–409, 1964.

Barr, S. L., III, R. R. N., Schultz, D. M., Stein, T. H. M., Abel, S. J., Baidu, M., Barrett, P. A., Bennett, L. J., Bland, J., Darlington, T., Gryspeerdt, E., Harvey, N. J., Lean, H. W., Lo, C. H. B., McQuaid, A., Norton, E. G., Osborne, S. R., Pickering, B. S., Rosenberg, P., Ricketts, H. M., Robinson, J., Thompson, R. J., Walden, C. J., Addison, F., Brooke, J. K., Clark, P., Clark, R., Daily, M. I., Fearn, A., Foster, P. B., Gray, S. L., Groves, J., Hanley, K. E., Kerr-Munslow, A., Keimer, J., Kumm, M., Langridge, J. M., Lin, J., Marker, L. R. R., McGregor, J. R., Moore, H., Murray, B. J., Price, J. D., Roberts, A. J., Scovell, R. W., Wellhausen, J., and Stirling, A. J.: The Wessex Convection Experiment (WesCon)–Observing the Evolving Structures of Turbulence (WOEST): coordinated aircraft and ground-based observations of turbulence and convection in southwest England during summer 2023, Geoscience Data Journal, https://doi.org/10.1002/gdj3.70092, accepted for publication, 2026.

Beck, J., Nuret, M., and Bousquet, O.: Model Wind Field Forecast Verification Using Multiple-Doppler Syntheses from a National Radar Network, Weather and Forecasting, 29, 331 – 348, https://doi.org/10.1175/WAF-D-13-00068.1, 2014.

Bell, M. M., Montgomery, M. T., and Emanuel, K. A.: Air–Sea Enthalpy and Momentum Exchange at Major Hurricane Wind Speeds Observed during CBLAST, Journal of the Atmospheric Sciences, 69, 3197 – 3222, https://doi.org/10.1175/JAS-D-11-0276.1, 2012.

Bousquet, O. and Tabary, P.: Development of a nationwide real-time 3-D wind and reflectivity radar composite in France, Quarterly Journal of the Royal Meteorological Society, 140, 611–625, https://doi.org/https://doi.org/10.1002/qj.2163, 2014.

Clark, P., Roberts, N., Lean, H., Ballard, S. P., and Charlton-Perez, C.: Convection-permitting models: a step-change in rainfall forecasting, Meteorological Applications, 23, 165–181, https://doi.org/https://doi.org/10.1002/met.1538, 2016.

Darlington, T.: Development, evaluation and applications of the Cyclops-DP Weather Radar Processing system, Phd thesis, University of Bath, 2015.

del Moral, A., Weckwerth, T. M., Rigo, T., Bell, M. M., and Llasat, M. C.: C-Band Dual-Doppler Retrievals in Complex Terrain: Improving the Knowledge of Severe Storm Dynamics in Catalonia, Remote Sensing, 12, https://doi.org/10.3390/rs12182930, 2020.

Fairman Jr, J. G., Schultz, D. M., Kirshbaum, D. J., Gray, S. L., and Barrett, A. I.: Climatology of size, shape, and intensity of precipitation features over Great Britain and Ireland, Journal of Hydrometeorology, 18, 1595–1615, 2017.

Field, P. R., Hill, A., Shipway, B., Furtado, K., Wilkinson, J., Miltenberger, A., Gordon, H., Grosvenor, D. P., Stevens, R., and Van Weverberg, K.: Implementation of a double moment cloud microphysics scheme in the UK met office regional numerical weather prediction model, Quarterly Journal of the Royal Meteorological Society, 149, 703–739, https://doi.org/https://doi.org/10.1002/qj.4414, 2023.

Gao, J., Xue, M., Shapiro, A., and Droegemeier, K. K.: A Variational Method for the Analysis of Three-Dimensional Wind Fields from Two Doppler Radars, Monthly Weather Review, 127, 2128 – 2142, https://doi.org/10.1175/1520-0493(1999)127<2128:AVMFTA>2.0.CO;2, 1999.

Gao, J., Xue, M., Brewster, K., and Droegemeier, K. K.: A Three-Dimensional Variational Data Analysis Method with Recursive Filter for Doppler Radars, Journal of Atmospheric and Oceanic Technology, 21, 457 – 469, https://doi.org/10.1175/1520-0426(2004)021<0457:ATVDAM>2.0.CO;2, 2004.

Gatlin, P. N., Petersen, W. A., Pippitt, J. L., Berendes, T. A., Wolff, D. B., and Tokay, A.: The GPM Validation Network and Evaluation of Satellite-Based Retrievals of the Rain Drop Size Distribution, Atmosphere, 11, https://doi.org/10.3390/atmos11091010, 2020.

https://doi.org/10.5194/egusphere-2026-4631
Preprint. Discussion started: 7 August 2026

Haase, G. and Landelius, T.: Dealiasing of Doppler Radar Velocities Using a Torus Mapping, Journal of Atmospheric and Oceanic Technology, 21, 1566 – 1573, https://doi.org/10.1175/1520-0426(2004)021<1566:DODRVU>2.0.CO;2, 2004.

Hanley, K. E., Plant, R. S., Stein, T. H., Hogan, R. J., Nicol, J. C., Lean, H. W., Halliwell, C., and Clark, P. A.: Mixing-length controls on high-resolution simulations of convective storms, Quarterly Journal of the Royal Meteorological Society, 141, 272–284, 2015.

Harrison, D. L., Scovell, R. W., and Kitchen, M.: High-resolution precipitation estimates for hydrological uses, in: Proceedings of the institution of civil engineers-water management, vol. 162, pp. 125–135, Thomas Telford Ltd, 2009.

Helmus, J. J. and Collis, S. M.: The Python ARM Radar Toolkit (Py-ART), a Library for Working with Weather Radar Data in the Python Programming Language, Journal of Open Research Software, https://doi.org/10.5334/jors.119, 2016.

Jackson, R., Collis, S., Lang, T., Potvin, C., and Munson, T.: PyDDA: A Pythonic Direct Data Assimilation Framework for Wind Retrievals, Journal of Open Research Software, 8, https://doi.org/10.5334/jors.264, 2020.

Lang, T. J., Potvin, C. K., Collis, S., Helmus, J., Jackson, R., Dolan, B., and Schultz, C.: Toward an Open-Source, Python-Powered, Multi-Doppler Radar Analysis Suite, in: American Meteorological Society Meeting Abstracts, vol. 97, pp. 4–4, 2017.

Lengfeld, K., Kirstetter, P.-E., Fowler, H. J., Yu, J., Becker, A., Flamig, Z., and Gourley, J.: Use of radar data for characterizing extreme precipitation at fine scales and short durations, Environmental Research Letters, 15, 085 003, 2020.

Lhermitte, R.: Dual-doppler observation of convective storm circulation, in: Proceedings of the 14th Radar Meteorology Conference, pp. 139–144, 1970.

Lhermitte, R. and Miller, L.: Doppler radar methodology for the observation of convective storms, in: Proceedings of the 14th Radar Meteorology Conference, pp. 133–138, 1970.

Liou, Y.-C. and Chang, Y.-J.: A Variational Multiple–Doppler Radar Three-Dimensional Wind Synthesis Method and Its Impacts on Thermodynamic Retrieval, Monthly Weather Review, 137, 3992 – 4010, https://doi.org/10.1175/2009MWR2980.1, 2009.

Lo, C. H. B., Stein, T. H. M., Scovell, R. W., Westbrook, C. D., Darlington, T., and Lean, H. W.: Use of ZDR columns for early detection of severe convection within the operational radar network of the United Kingdom, Meteorological Applications, 31, e2159, https://doi.org/https://doi.org/10.1002/met.2159, 2024.

Louf, V., Protat, A., Jackson, R. C., Collis, S. M., and Helmus, J.: UNRAVEL: A Robust Modular Velocity Dealiasing Technique for Doppler Radar, Journal of Atmospheric and Oceanic Technology, 37, 741 – 758, https://doi.org/10.1175/JTECH-D-19-0020.1, 2020.

Met Office: Met Office Rain Radar Data from the NIMROD System, https://catalogue.ceda.ac.uk/uuid/82adec1f896af6169112d09cc1174499/, accessed 31 July 2026, 2003.

Mittermaier, M. P.: A Strategy for Verifying Near-Convection-Resolving Model Forecasts at Observing Sites, Weather and Forecasting, 29, 185 – 204, https://doi.org/10.1175/WAF-D-12-00075.1, 2014.

Neely III, R. R., Bennett, L., Blyth, A., Collier, C., Dufton, D., Groves, J., Walker, D., Walden, C., Bradford, J., Brooks, B., Addison, F. I., Nicol, J., and Pickering, B.: The NCAS mobile dual-polarisation Doppler X-band weather radar (NXPol), Atmospheric Measurement Techniques, 11, 6481–6494, https://doi.org/10.5194/amt-11-6481-2018, 2018.

Nicol, J., Hogan, R., Stein, T., Hanley, K., Clark, P., Halliwell, C., Lean, H., and Plant, R.: Convective updraught evaluation in high-resolution NWP simulations using single-Doppler radar measurements, Quarterly Journal of the Royal Meteorological Society, 141, 3177–3189, 2015.

North, K. W., Oue, M., Kollias, P., Giangrande, S. E., Collis, S. M., and Potvin, C. K.: Vertical air motion retrievals in deep convective clouds using the ARM scanning radar network in Oklahoma during MC3E, Atmospheric Measurement Techniques, 10, 2785–2806, https://doi.org/10.5194/amt-10-2785-2017, 2017.

https://doi.org/10.5194/egusphere-2026-4631
Preprint. Discussion started: 7 August 2026

Norton, E., Vaughan, G., Methven, J., Coe, H., Brooks, B., Gallagher, M., and Longley, I.: Boundary layer structure and decoupling from synoptic scale flow during NAMBLEX, Atmospheric Chemistry and Physics, 6, 433–445, 2006.

Pauley, P. M. and Wu, X.: The Theoretical, Discrete, and Actual Response of the Barnes Objective Analysis Scheme for One- and Two-Dimensional Fields, Monthly Weather Review, 118, 1145 – 1164, https://doi.org/10.1175/1520-0493(1990)118<1145:TTDAAR>2.0.CO;2, 1990.

Petersen, G. N. and Renfrew, I. A.: Aircraft-based observations of air–sea fluxes over Denmark Strait and the Irminger Sea during high wind speed conditions, Quarterly Journal of the Royal Meteorological Society, 135, 2030–2045, https://doi.org/https://doi.org/10.1002/qj.355, 2009.

Potvin, C. K., Betten, D., Wicker, L. J., Elmore, K. L., and Biggerstaff, M. I.: 3DVAR versus Traditional Dual-Doppler Wind Retrievals of a Simulated Supercell Thunderstorm, Monthly Weather Review, 140, 3487 – 3494, https://doi.org/10.1175/MWR-D-12-00063.1, 2012a.

Potvin, C. K., Shapiro, A., and Xue, M.: Impact of a Vertical Vorticity Constraint in Variational Dual-Doppler Wind Analysis: Tests with Real and Simulated Supercell Data, Journal of Atmospheric and Oceanic Technology, 29, 32 – 49, https://doi.org/10.1175/JTECH-D-11-00019.1, 2012b.

Powers, J. G., Klemp, J. B., Skamarock, W. C., Davis, C. A., Dudhia, J., Gill, D. O., Coen, J. L., Gochis, D. J., Ahmadov, R., Peckham, S. E., Grell, G. A., Michalakes, J., Trahan, S., Benjamin, S. G., Alexander, C. R., Dimego, G. J., Wang, W., Schwartz, C. S., Romine, G. S., Liu, Z., Snyder, C., Chen, F., Barlage, M. J., Yu, W., and Duda, M. G.: The Weather Research and Forecasting Model: Overview, System Efforts, and Future Directions, Bulletin of the American Meteorological Society, 98, 1717 – 1737, https://doi.org/10.1175/BAMS-D-15-00308.1, 2017.

Ribaud, J.-F., Bousquet, O., and Coquillat, S.: Relationships between total lightning activity, microphysics and kinematics during the 24 September 2012 HyMeX bow-echo system, Quarterly Journal of the Royal Meteorological Society, 142, 298–309, https://doi.org/https://doi.org/10.1002/qj.2756, 2016.

Roberts, N. M., Cole, S. J., Forbes, R. M., Moore, R. J., and Boswell, D.: Use of high-resolution NWP rainfall and river flow forecasts for advance warning of the Carlisle flood, north-west England, Meteorological Applications: A journal of forecasting, practical applications, training techniques and modelling, 16, 23–34, 2009.

Schär, C., Fuhrer, O., Arteaga, A., Ban, N., Charpilloz, C., Girolamo, S. D., Hentgen, L., Hoefler, T., Lapillonne, X., Leutwyler, D., Osterried, K., Panosetti, D., Rüdisühli, S., Schlemmer, L., Schulthess, T. C., Sprenger, M., Ubbiali, S., and Wernli, H.: Kilometer-Scale Climate Models: Prospects and Challenges, Bulletin of the American Meteorological Society, 101, E567 – E587, https://doi.org/10.1175/BAMS-D-18-0167.1, 2020.

Scovell, R. and Al-Sakka, H.: A point cloud method for retrieval of high-resolution 3D gridded reflectivity from weather radar networks for air traffic management, Journal of Atmospheric and Oceanic Technology, 33, 461–479, 2016.

Shapiro, A., Potvin, C. K., and Gao, J.: Use of a Vertical Vorticity Equation in Variational Dual-Doppler Wind Analysis, Journal of Atmospheric and Oceanic Technology, 26, 2089 – 2106, https://doi.org/10.1175/2009JTECHA1256.1, 2009.

Skamarock, W. C., Klemp, J. B., Dudhia, J., Gill, D. O., Liu, Z., Berner, J., Wang, W., Powers, J. G., Duda, M. G., Barker, D. M., et al.: A description of the advanced research WRF version 4, NCAR tech. note ncar/tn-556+ str, 145, 2019.

Sproson, D. A. J.: FAAM core data product documentation, https://doi.org/10.5281/zenodo.14508958, 2024.

Stein, T. H. M., Hogan, R. J., Hanley, K. E., Nicol, J. C., Lean, H. W., Plant, R. S., Clark, P. A., and Halliwell, C. E.: The Three-Dimensional Morphology of Simulated and Observed Convective Storms over Southern England, Monthly Weather Review, 142, 3264 – 3283, https://doi.org/10.1175/MWR-D-13-00372.1, 2014.

https://doi.org/10.5194/egusphere-2026-4631
Preprint. Discussion started: 7 August 2026

Stein, T. H. M., Hogan, R. J., Clark, P. A., Halliwell, C. E., Hanley, K. E., Lean, H. W., Nicol, J. C., and Plant, R. S.: The DYMECS Project: A Statistical Approach for the Evaluation of Convective Storms in High-Resolution NWP Models, Bulletin of the American Meteorological Society, 96, 939 – 951, https://doi.org/10.1175/BAMS-D-13-00279.1, 2015.

Stein, T. H. M., Scovell, R. W., Hanley, K. E., Lean, H. W., and Marsden, N. H.: The potential use of operational radar network data to evaluate the representation of convective storms in NWP models, Quarterly Journal of the Royal Meteorological Society, 146, 2315–2331, https://doi.org/https://doi.org/10.1002/qj.3793, 2020.

Tsai, C.-L., Kim, K., Liou, Y.-C., and Lee, G.: High-resolution 3D winds derived from a modified WISSDOM synthesis scheme using multiple Doppler lidars and observations, Atmospheric Measurement Techniques, 16, 845–869, https://doi.org/10.5194/amt-16-845-2023, 2023.

Westbrook, C. and Clark, M.: Observations of a tornadic supercell over Oxfordshire using a pair of Doppler radars, Weather, 68, 128–134, https://doi.org/https://doi.org/10.1002/wea.1997, 2013.